

Spin model for the Honeycomb NiPS₃

Paula Mellado¹

School of Engineering and Sciences, Universidad Adolfo Ibáñez, Santiago, Chile

(*Electronic mail: paula.mellado@uai.cl)

(Dated: 14 December 2023)

In the Van der Waal material NiPS₃, Ni atoms have spin $S=1$ and realize a honeycomb lattice. Six sulfur atoms surround each Ni and split their d manifold into three filled and two unfilled bands. Aimed to determine the spin Hamiltonian of NiPS₃, we study its exchange mechanisms using a two-band half-filled Hubbard model. Hopping between d orbitals is mediated by p orbitals of sulfur and gives rise to bilinear and biquadratic spin couplings in the limit of strong electronic correlations. The microscopic model exposed a ferromagnetic biquadratic spin interaction K_1 allowing the completion of a minimal $J_1 - J_3 - K_1$ spin Hamiltonian for NiPS₃. In bulk, a ferromagnetic first nearest neighbor J_1 and a more significant antiferromagnetic third nearest neighbor spin coupling J_3 agreed with the literature, while in monolayer J_1 is positive and very small in comparison. Using a variational scheme we found that a zig-zag antiferromagnetic order is the ground state of bulk samples. The zig-zag pattern is adjacent to commensurate and incommensurate spin spirals, which could hint at the puzzling results reported in NiPS₃ monolayers.

Van der Waal compounds, particularly transition-metal thiophosphates¹, are an exciting class of materials. Their negligible interlayer coupling reduces their dimensionality and promotes intriguing electronic and optical quantum effects²⁻¹⁵ while allowing for easy tunability of magnetic exchange and anisotropy through ligand substitution^{16,17}. Family members of transition-metal thiophosphates Van der Waal materials have monoclinic space group $C/2m$, with the transition metal atoms forming a planar honeycomb lattice in the ab planes¹⁸, Fig.1(a). The metal atoms are enclosed in octahedra formed by sulfur atoms and have a phosphorus doublet at the center of the honeycomb hexagons^{19,20}. Magnetic susceptibility measurements on single crystals reveal that the family mem-

ber NiPS₃ has the smallest spin $S = 1$ ²³ and the largest Neel temperature $T_N = 155$ K. Experimental measurements^{3,23-27} and DFT calculations^{18,24,25,28-31} show that below T_N Ni spins form a zig-zag antiferromagnetic ground state featured as double parallel ferromagnetic chains antiferromagnetically coupled within the single layer (see Fig.1). Large spacing between adjacent layers suppresses interlayer exchange such that the antiferromagnetic order acquires a 2D character even in the bulk form²⁴. Spin dynamics in NiPS₃ has been proved by high-resolution spectroscopy methods^{24,32}, and linear spin-wave theory using a Heisenberg Hamiltonian with single-ion anisotropies was applied to determine the magnetic exchange parameters and the nature of the anisotropy in NiPS₃ samples^{18,23,33}. In-plane magnetic exchange interactions up to third-nearest neighbors were required to account for the results. The nearest-neighbor exchange was found ferromagnetic with $J_1 \sim 2.5$ meV and the dominant antiferromagnetic third-neighbor exchange $J_3 \sim 13$ meV. Both, XY-like anisotropy and a small uniaxial component were required to fit the experimental results which led to two low-energy spin wave modes appearing in the spin-wave spectrum at the Brillouin zone center²⁵. The anisotropic Heisenberg Hamiltonian with up to three nearest neighbor couplings could reproduce the spin-wave energies but was at odds with the calculated neutron intensities showing that the classical spin models accounting for its magnetism up to date are a subject of debate.^{23,24,26,28,29,34} Further, the presence of orbital degeneracy combined with the small magnitude of Ni spins suggests that quantum aspects could play a role in the magnetic properties of NiPS₃.

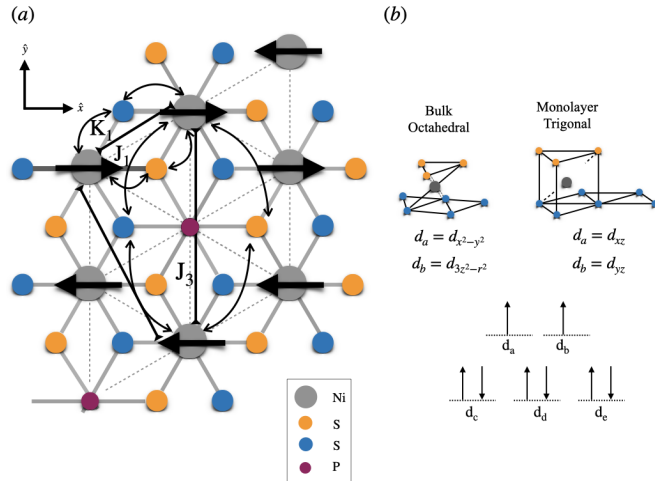


FIG. 1. (a) Top view of a single layer of NiPS₃. Grey, blue, orange, and cyan-filled circles illustrate Ni, top Sulfur, bottom Sulfur, and P atoms. Black arrows on top of grey circles illustrate the direction of spins in Ni atoms when the system is in the zig-zag magnetic state. Curved arrows highlight superexchange between Ni atoms mediated by sulfur ions. J_1 , J_3 , and K_1 denote the first and third nearest neighbor and biquadratic first nearest neighbor spin couplings, respectively. (b) Crystal field in bulk and monolayer and the splitting of the d band^{21,22}.

Aimed to find the spin model responsible for the magnetism in NiPS₃, here we study the electron exchange mechanisms of a multi-band Hubbard model for the Ni atoms in NiPS₃ in the limit of strong Coulomb interactions. d orbitals in transition-metals are localized, and direct exchange hopping can only occur between orbitals on different atoms that are very close to each other³⁵, which makes direct hopping unlikely in NiPS₃. Therefore the exchange mechanisms are extended by taking into account hopping via intermediate p orbitals located at the sulfur atoms in between two Ni sites. Integrating out the

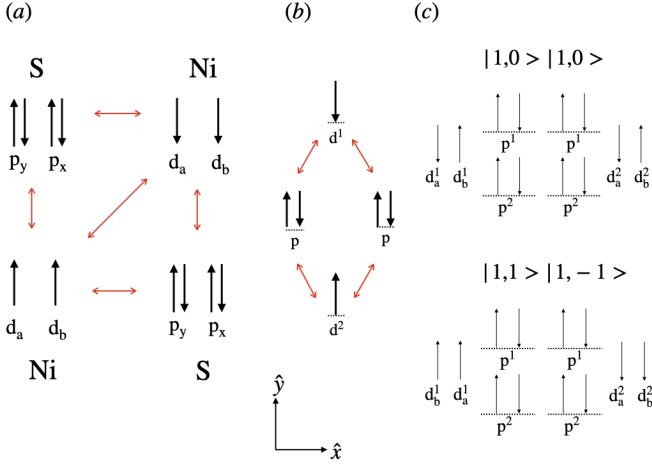


FIG. 2. Proposed superexchange mechanism between (a) nearest neighbors d orbitals in NiPS₃ and (b) third nearest neighbors. (c) Two initial spin states with total spin S=1.

high energy states of the microscopic model, spin exchanges were computed. Besides ferromagnetic and antiferromagnetic bilinear spin interactions, we found that a ferromagnetic biquadratic spin coupling is important in NiPS₃, giving rise to the following bilinear-biquadratic effective spin Hamiltonian for the Ni atoms:

$$\begin{aligned} \mathcal{H} = & -J_1 \sum_{\langle ij \rangle} (\mathbf{S}_i \cdot \mathbf{S}_j) + J_3 \sum_{\langle ik \rangle} (\mathbf{S}_i \cdot \mathbf{S}_k) \\ & - K_1 \sum_{\langle ij \rangle} (\mathbf{S}_i \cdot \mathbf{S}_j)^2 \end{aligned} \quad (1)$$

where J_1 and J_3 denote the first and third nearest neighbor spin exchange couplings, respectively, and K_1 is the first neighbor biquadratic spin exchange. The computed spin couplings are shown in Table I and were used to evaluate the system's variational ground state energy considering the quantum nature of spins in NiPS₃. We found that the zig-zag magnetic order corresponds to the ground state of Eq.1 in the relevant space of parameters for bulk NiPS₃¹⁸. The zig-zag pattern coexists with a ferroquadrupolar order and competes with magnetic commensurate and incommensurate magnetic spirals. In monolayer NiPS₃, trigonal distortions²⁶ found in experimental samples, change J_1 to smaller and antiferromagnetic values which could drive monolayers to a Neel magnetic phase¹⁸.

In bulk NiPS₃ the octahedral crystal field at Ni sites causes the 3d orbitals to split into a triplet of lower energy, d_{xy} , d_{xz} , d_{yz} and a doublet $d_{x^2-y^2}$, $d_{3z^2-r^2}$, Fig1(b)^{21,22,32,36}. Each Ni²⁺ is in a d⁸ electronic configuration. Consequently, d orbitals belonging to the triplet are fully occupied while the doublet is half filled. While bulk samples have a monoclinic structure with point group C_{2h} , monolayers have a hexagonal structure with point group D_{3d} ³. In monolayers, due to trigonal distortions²⁶ the crystal field splits d orbitals into the fully occupied triplet $d_{x^2-y^2}$, $d_{3z^2-r^2}$, d_{xy} , and the doublet d_{xz} , d_{yz} ^{12,15,19,37}. Consider the case of two atoms of Ni with two d orbitals, each forming a spin S=1 state, and two

atoms of sulfur symmetrically located in between the Ni and with two fully occupied p orbitals, Fig.2(a). Operator $c_{i\alpha\sigma}^\dagger$ creates a spin electron $\sigma = \uparrow, \downarrow$ in the α orbital at site i and $n_{i,\alpha,\sigma} = c_{i\alpha\sigma}^\dagger c_{i\alpha\sigma}$ defines the number of electrons at site i and orbital α with spin σ . The difference in energy of p and d orbitals is denoted Δ ^{13,21}. Onsite Coulomb repulsion of two electrons in a single d orbital is U_d ; electron repulsion in p orbitals is neglected. The transfer of one electron from p to d orbital has associated the energy $U = U_d + \Delta$. $t_{\alpha\beta}^{ij}$ denotes the hopping amplitude from orbital α at site i to orbital β at site j . Intrasite orbital hopping cancels since orbitals at the same site are orthogonal. States of interest have a fixed magnetic moment $S = 1$ per site (atom). Interband charge interactions are considered, therefore Hund's couplings J_H and J'_H are included at Ni and sulfur sites respectively²². Altogether the microscopic model^{38,39} becomes:

$$\begin{aligned} H = & \sum_{\substack{i \neq j \\ \alpha \neq \beta}} t_{\alpha\beta}^{ij} (c_{i\alpha\sigma}^\dagger c_{j\beta\sigma} + H.c.) \\ & + U \sum_{i,\alpha} n_{i\alpha\uparrow} n_{i\alpha\downarrow} - J_H \sum_{i,\sigma,\alpha \neq \beta} n_{i\alpha\sigma} n_{i\beta\sigma} \\ & - J'_H \sum_{i,\alpha \neq \beta} (c_{i\alpha\uparrow}^\dagger c_{i\alpha\downarrow} c_{i\beta\downarrow}^\dagger c_{i\beta\uparrow} + H.c.) \end{aligned} \quad (2)$$

In NiPS₃ the spin exchange at the nearest neighbor level results from a competition between direct overlap of d orbitals and indirect hopping mediated by sulfur atoms⁴⁰. In the direct process, electrons hop between Ni orbitals at different sites of the honeycomb lattice. The indirect exchange mechanism known as superexchange^{22,41,42} is mediated by the virtual hopping to two sulfur ions in between the two Ni atoms. This is a more realistic situation for NiPS₃ because in transition metals compounds, the overlap between d orbitals³⁵ separated a distance r decays as $\sim 1/r^5$. Consider the two initial states of Fig.2(c) where spins at different Ni sites are antiparallel. They are denoted $|1,0\rangle |1,0\rangle$ and $|1,1\rangle |1,-1\rangle$, according to the notation $|S^1, m^1\rangle |S^2, m^2\rangle$ where S^k and m^k represent respectively the total spin quantum number of site k and the z component of the total spin. With four available half-filled d-orbitals, up to four electrons could hop. The electron hopping from the initial states with $S^k = 1$ gives rise to intermediate states with one, two, three, and four double-occupied d-orbitals where $S^k \neq 1$. Indirect interactions across intermediate states mediate interactions between $|1,0\rangle |1,0\rangle$ and $|1,1\rangle |1,-1\rangle$. To integrate out high energy states, the electron Hamiltonian matrix from Eq.2 was separated into $H = \tilde{H}_{0,0} + \tilde{H} + \tilde{T}$. $\tilde{H}_{0,0}$ and \tilde{H} contain the on-site contributions due to Coulomb interactions and interband charge interactions of the low-energy states with no double occupied d orbitals, ($\tilde{H}_{0,0}$), and the high energy states with at least one double occupied d-orbital (\tilde{H}). \tilde{T} contains off-diagonal terms due to electron hopping (details in Supplementary Material). H was partitioned into blocks where diagonal matrices contain the energy of the basis states with k double occupied d-orbitals ($\tilde{H}_{k,k}$). Off diagonal blocks are hopping matrices $\tilde{T}_{k-1,k}$ that connect states with $k-1$ and

J_1^s	$-\frac{t_{pd}^4 J_H^2 (J_H - 2U)^2}{2U^4 (J_H - U)^2}$
J_1^D	$\frac{t_{dd}^2 (J_H - 2U_d)}{U (J_H - U_d)}$
J_3	$\frac{t_{pd}^4 \left(\frac{1}{U_d} + \frac{1}{(U_d + \Delta)} \right) \frac{4}{(U_d + \Delta)^2}}{(U_d + \Delta)^2}$
K_1	$-2J_H^s \left[t_{pd}^6 \frac{(16J_H^2 - 63J_H U + 72U^2)}{18U^6 (J_H - U)^2} + t_{pd}^8 \frac{(47J_H - 108U)(5J_H - 12U)}{864U^8 (J_H - U)^2} \right]$

TABLE I. Spin couplings for spins in Ni atoms of NiPS₃ computed from direct and superexchange processes in Eq.2.

NiPS ₃	Monolayer	Bulk
t_{dd}	$t_{d_{xz}d_{xz}} \sim t_{dd}\pi$ $t_{d_{yz}d_{yz}} \sim t_{dd}\pi$	$t_{d_{x^2-y^2}d_{x^2-y^2}} \sim t_{dd}\pi$ $t_{d_{3z^2-r^2}d_{3z^2-r^2}} \sim \frac{1}{4}t_{dd}\sigma$
t_{pd}	$t_{d_{xz}p_x} \sim t_{pd}\pi$ $t_{d_{yz}p_x} \sim t_{pd}\pi$ $t_{d_{xz}p_y} \sim t_{pd}\pi$ $t_{d_{yz}p_y} \sim t_{pd}\pi$	$t_{d_{x^2-y^2}p_x} \sim \frac{\sqrt{3}}{2}t_{pd}\sigma$ $t_{d_{3z^2-r^2}p_x} \sim \frac{1}{2}t_{pd}\sigma$ $t_{d_{x^2-y^2}p_y} \sim \frac{\sqrt{3}}{2}t_{pd}\sigma$ $t_{d_{3z^2-r^2}p_y} \sim \frac{1}{2}t_{pd}\sigma$
J_1^D	5×10^{-4}	5×10^{-4}
J_1^s	-2×10^{-4}	-2×10^{-3}
$J_1 = J_1^D + J_1^s$	3×10^{-4}	-1×10^{-3}
K_1/J_1	-7×10^{-3}	1×10^{-2}
J_3/J_1	1.2	-3

TABLE II. Slater-Koster integrals between d and between p and d-orbitals from ref.³⁵. Approximate numerical evaluation (in [eV] units) of the spin couplings presented in Table I in bulk and monolayer of NiPS₃ using parameters for NiPS₃ from the literature^{18,29,37} such as $U=6$ [eV] $J_H = J_H' = 0.7$ [eV], $\Delta = 3$ [eV], $t_{dd} = 0.05$ [eV], $t_{pd\sigma} = 1$ [eV].

k double occupied d-orbitals:

$$H = \begin{pmatrix} \tilde{H}_{0,0} & \tilde{T}_{0,1} & \tilde{0} & \tilde{0} & \tilde{0} \\ \tilde{T}_{1,0} & \tilde{H}_{1,1} & \tilde{T}_{1,2} & \tilde{0} & \tilde{0} \\ \tilde{0} & \tilde{T}_{2,1} & \dots & \dots & \dots \\ \tilde{0} & \tilde{0} & \dots & \tilde{H}_{k-1,k-1} & \tilde{T}_{k-1,k} \\ \tilde{0} & \tilde{0} & \dots & \tilde{T}_{k,k-1} & \tilde{H}_{k,k} \end{pmatrix}$$

The subspaces are decoupled through a canonical transformation using the perturbative approach of Löwdin⁴³ and Schrieffer-Wolff^{44,45} where \tilde{H} and \tilde{T} are treated as perturbation (see Supplementary Material). In this way, high energy states are down-folded into the energetically well-separated sector of interacting spins of constant quantum number at each site²². This is a consequence of Hund's coupling and onsite Coulomb interactions, which are large with respect to the hopping amplitudes in transition metal compounds⁴⁶. For nearest neighbor Ni atoms (1-nn), sulfur ions form a ninety degrees bridge between the two Ni sites, Fig.1(a) and Fig.2(a)^{19,22,35}. By symmetry, there is only hopping between d and p orbitals that point to each other. Therefore in the superexchange process at 1-nn level at each Ni site, one of the d-orbitals could overlap with the p_x orbital of one of the sulfur atoms, and the other could overlap with the p_y orbital of the second, Fig.2(a). The superexchange Hamiltonian matrix contains five diagonal blocks with the energy of: the two initial states, $\tilde{H}_{0,0}$, the eight excited states with one double occupied d-orbital, $\tilde{H}_{1,1}$,

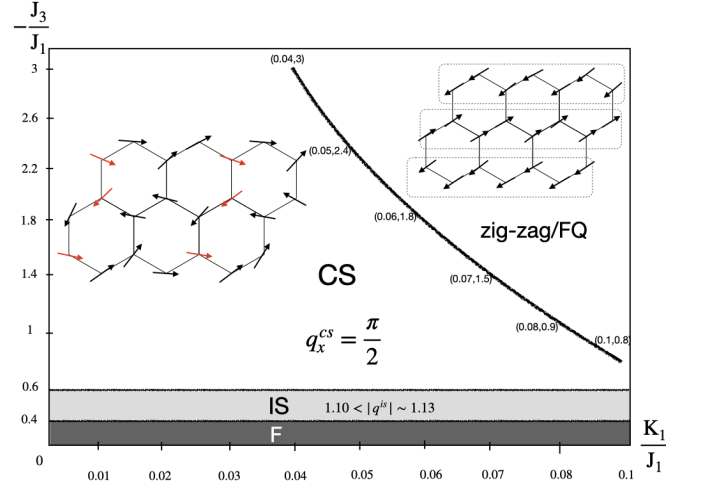


FIG. 3. Variational phase diagram of Eq.1, at $T=0$. Arrows in red illustrate periodicity of spins in the spiral phase CS.

the twelve states with two double occupied d-orbitals, $\tilde{H}_{2,2}$, the eight with three double occupied d-orbitals, $\tilde{H}_{3,3}$, and the two excited states with four double occupied d-orbitals, $\tilde{H}_{4,4}$. The off diagonal matrix elements consist of hopping matrices ($\tilde{T}_{0,1}$, $\tilde{T}_{1,2}$, $\tilde{T}_{2,3}$, $\tilde{T}_{3,4}$) between the basis states. Though expected to be small, direct exchange between 1-nn is also considered here. Second neighbors Ni atoms (2-nn) do not share a common sulfur ion in NiPS₃, (Fig.1); therefore, the electron exchange proceeds via direct overlap, which for 2-nn is neglected. In the case of third nearest neighbor Ni atoms (3-nn), the angle between two 3-nn Ni and the two sulfur ions in between is larger than ninety degrees, Fig.1. Consequently, superexchange between two 3-nn Ni could be mediated by a single p orbital²², which serves the two Ni ions, Fig.2(b). At 3-nn level, direct exchange is neglected and we only consider bilinear spin exchanges; therefore, only virtual hopping of one and two electrons are computed.

Downfolding the high energy states by going up to fourth order in perturbation theory⁴³⁻⁴⁵ and by writing spin operators in terms of electron operators $c_{i\alpha\sigma}$, $c_{i\alpha\sigma}^\dagger$ yields the effective spin Hamiltonian of the electron system (as shown in the Supplementary Material). Mediated by two orthogonal p orbitals, the spin couplings $J_1^s < 0$ and $K_1 < 0$ are ferromagnetic, and they correspond respectively to bilinear and biquadratic 1-nn spin interactions originated from four, six and eight virtual hoppings. J_1^D originates from a direct exchange between Ni atoms and is antiferromagnetic. $J_3 > 0$ originates from four virtual hopping mediated by a single p orbital and consequently is antiferromagnetic^{22,42}. Explicit expressions for $J_1 = J_1^s + J_1^D$, J_3 and K_1 are shown in Table I. There, terms $\mathcal{O}(t_{pd}^4)$ arise from two double occupied d-orbitals. Terms proportional to $\mathcal{O}(t_{pd}^6)$ correspond to three double occupied d-orbitals from six p-d hopping processes, and the term $\mathcal{O}(t_{pd}^8)$ accounts for four double occupied d-orbitals. Terms proportional to $\mathcal{O}(t_{dd}^2)$ are due to one doubly occupied d-orbital due to direct exchange.

While in bulk NiPS₃ the octahedral crystal field favors the

doublet $d_{x^2-y^2}, d_{3z^2-r^2}$, in monolayers the trigonal distortion of such a field²⁶ favors the doublet d_{xz}, d_{yz} , Fig.1(b)^{15,22,35}. Even though the trigonal distortion could change the angles between Ni and S atoms^{15,22,35} here we neglect this important effect and assume that the different symmetry of the participating d-orbitals in bulk and monolayer does not change the superexchange mechanism presented above; however, it affects the values of the hopping integrals according to the Slater-Koster scheme^{35,47} as shown in Table II. Taking into account the Slater-Koster rules, considering all possible combinations of d and p orbital hopping³⁵ and using values of U, Δ and J_H from the literature³⁷ the spin couplings from Table I in bulk and monolayer NiPS₃ are evaluated and shown in Table II. We find that in the case of bulk samples $|J_1^D| < |J_1^S|$.

To study magnetic orders of Eq.1 at T=0, we consider the trial ground state $|\psi\rangle = \otimes_i |\psi_i\rangle$ ^{13,48,49}. It consists of an entanglement-free direct product of arbitrary wavefunctions with spin S=1 at each site^{48,50}. A general single spin state can be written as the coherent state

$$|\psi_i\rangle = b_{ix}|x\rangle + b_{iy}|y\rangle + b_{iz}|z\rangle \quad (3)$$

where \mathbf{b}_i is an arbitrary complex vector satisfying the normalization constraint $\mathbf{b}_i^* \cdot \mathbf{b}_i = \mathbf{1}$, and we have chosen the time-reversal invariant basis of the $SU(3)$ (S=1) fundamental representation $|x\rangle = \frac{i|1\rangle - i|\bar{1}\rangle}{\sqrt{2}}$, $|y\rangle = \frac{i|1\rangle + i|\bar{1}\rangle}{\sqrt{2}}$, $|z\rangle = -i|0\rangle$ where $|1\rangle, |\bar{1}\rangle$ and $|0\rangle$ are the three cartesian spin-1 states quantized along the z axis⁴⁹. The basis states satisfy $S^x|x\rangle = S^y|y\rangle = S^z|z\rangle = 0$. The magnetization of the system is defined through the expectation value of the spin at each site⁵⁰

$$M = \sum_k \langle \psi_k | \mathbf{S}_k | \psi_k \rangle = -i \sum_k \mathbf{b}_k^* \times \mathbf{b}_k \quad (4)$$

In terms of the complex vectors \mathbf{b}_i the expectation value of the $J_1 - J_3 - K_1$ spin Hamiltonian of Eq.1 becomes

$$\begin{aligned} \langle \psi | \mathcal{H} | \psi \rangle &= \sum_{\langle ij \rangle} \left[-J_1 |\mathbf{b}_i^* \cdot \mathbf{b}_j|^2 + (J_1 - K_1) |\mathbf{b}_i \cdot \mathbf{b}_j|^2 \right] \\ &+ J_3 \sum_{(ij)} \left[|\mathbf{b}_i^* \cdot \mathbf{b}_j|^2 - |\mathbf{b}_i \cdot \mathbf{b}_j|^2 \right] \end{aligned} \quad (5)$$

Because of the biquadratic interaction, we investigate a possible quadrupolar order, QP in the system⁵⁰. To that purpose we introduce the quadrupolar operator QP, a tensor with five components $\mathbf{Q}_i = [Q_i^{x^2-y^2}, Q_i^{3z^2-r^2}, Q_i^{xy}, Q_i^{yz}, Q_i^{xz}] = [(S_i^x)^2 - (S_i^y)^2, (2(S_i^z)^2 - (S_i^x)^2 - (S_i^y)^2)/\sqrt{3}, S_i^x S_i^y + S_i^y S_i^x, S_i^y S_i^z + S_i^z S_i^y, S_i^x S_i^z + S_i^z S_i^x]$. QP can be expressed in terms of the complex \mathbf{b} vectors,

$$\langle \psi_i | \mathbf{Q}_{\mu,\nu} | \psi_i \rangle = \frac{1}{3} \delta_{\mu,\nu} - \frac{1}{2} (b_{i\mu}^* b_{i\nu} + b_{i\nu}^* b_{i\mu}) \quad (6)$$

Using the identity $\mathbf{Q}_i \cdot \mathbf{Q}_j = 2(\mathbf{S}_i \cdot \mathbf{S}_j)^2 + \mathbf{S}_i \cdot \mathbf{S}_j - 2/3$, in terms of the QP operators the $J_1 - J_3 - K_1$ Hamiltonian, Eq.1 can be written as:

$$\begin{aligned} \mathcal{H} &= -(J_1 - \frac{K_1}{2}) \sum_{\langle ij \rangle} (\mathbf{S}_i \cdot \mathbf{S}_j) + J_3 \sum_{(ik)} (\mathbf{S}_i \cdot \mathbf{S}_k) \\ &- \frac{K_1}{2} \sum_{\langle ij \rangle} (\mathbf{Q}_i \cdot \mathbf{Q}_j) - \sum_i \frac{4}{3} K \end{aligned} \quad (7)$$

To find variational ground states of the spin Hamiltonian Eq.1, the variational Eq.5 was minimized respect to all complex \mathbf{b}_i vectors in a hexagonal cluster of twenty-two spins (as the one shown in the inset of Fig.3) by using the *Nminimize* procedure from Wolfram Mathematica⁵¹ (see Supplementary Material). Fig.3 presents the corresponding $-J_3/J_1$ v/s K_1/J_1 phase diagram of Eq.1 at T=0. We considered ferromagnetic nearest neighbour couplings and antiferromagnetic J_3 in the range of results valid for bulk samples, given in Tables I and II. Four magnetic phases and one quadrupolar order have been identified. For all values of K_1 and for J_3 in the range $0 \leq |J_3| \leq 0.4J_1$ the system settles in a ferromagnetic state F, but as J_3 enters in the range $0.4J_1 \leq |J_3| \leq 0.6J_1$ spins rearrange into incommensurate spirals IS out of the $x - y$ plane. For $J_3 \geq 0.6J_1$ two magnetic phases can arise. At $K_1 > 0.4J_1$ a zig-zag phase with spins canted out of the $x - y$ plane competes with a commensurate spiral magnetic order CS with wavevector $\mathbf{q}_x^{cs} = \frac{2\pi}{3}$. The zig-zag phase with zero average spin moment coexists with a uniaxial ferroquadrupolar order FQ⁵⁰. The CS order (inset of Fig.3) is a noncoplanar spiral where generally spins settle out of the $x - y$ plane and give rise to non zero QP moments^{48,50}. Magnetic phases and quadrupolar order were identified by inspecting the ground state spin textures obtained from the variational results and were confirmed by computing the space correlation functions through the static structure factor of the magnetization and quadrupolar order parameters $C, S(\mathbf{q}) = e^{i\mathbf{r}_i \cdot \mathbf{q}} \langle \mathbf{C}_i \cdot \mathbf{C}_j \rangle$ for $q \in (0, \pi)$ (as shown in the Supplementary Material). Phase boundaries were identified by computing the second derivative of the ground state energy, with respect to the couplings J_3 and K_1 , and looking for singular features indicative of changes in the ground state phases.

Quadrupolar and spin correlations grow toward larger values of K_1/J_1 , and from IS, toward larger values of $|J_3/J_1|$. Inspecting Eq.7, in the case of $J_3 = 0$ a ferromagnetic ground state is expected as long as $|J_1| > \frac{|K_1|}{2}$. Variational results show that increasing K_1 drives the spins in CS toward a coplanar spiral phase until the system reaches the collinear zig-zag state.

For $J_3 \geq 0$ and $(J_1 - \frac{K_1}{2}) > 0$ magnetic frustration could lead the system to disordered phases. But if J_3 is large enough, the zig-zag state is favoured where a single spin is arranged ferromagnetically with two of the nearest neighbors in its chain and antiferromagnetically with the third one in a next neighbor chain. Nevertheless, the zig-zag state becomes more difficult to accomplish as J_3 and K_1 approach the limit $|J_1 - \frac{K_1}{2}| \sim |J_3|$. In this case our variational calculations show that the IS phase arises.

To further investigate the spiral order in bulk NiPS₃, we introduced the ansatz $\mathbf{b}_i = (\sin \theta \cos(\mathbf{q} \cdot \mathbf{r}_i) e^{i\phi}, \sin \theta \sin(\mathbf{q} \cdot \mathbf{r}_i) e^{i\phi}, \cos \theta)$ ⁵⁰ for the vector of amplitudes \mathbf{b}_i describing the wavefunction at a single site located at position \mathbf{r}_i in the honeycomb lattice. Now Eq.5 was minimized with respect to \mathbf{q}, θ, ϕ in the hexagonal cluster with twenty-two spins introduced before, and the results were compared with the variational ones confirming zig-zag, F, and QP orders, as well as the wavevector $\mathbf{q}_x^{cs} = 2\pi/3$. In the range of parameters of IS we found the order wavevector

$$1.10 < |\mathbf{q}^{is}| \sim 1.15.$$

Previous studies have reported that the orientation of magnetic moments in NiPS₃ could be influenced by biaxial magnetocrystalline anisotropy consisting of a dominant easy-plane anisotropy that locks the orientation of the spins to a magnetic plane $x-y$ slightly inclined from the crystallographic ab plane, and a secondary weaker anisotropy that orients the spins in the magnetic $x-y$ plane along the x -axis^{18,23}. To determine its effects on the phase diagram of Fig.3 the term $A \sum_j (S_j^z)^2 = A \sum_j [i(\mathbf{b}_j^* \times \mathbf{b}_j) \cdot \hat{\mathbf{z}}]^2$ was added to Eq.1, where A plays the role of the anisotropic coupling. Variational ground states were subsequently computed for the range of parameters of Fig.3 and $0 \leq A \leq 2 \times 10^{-1} J_1$ according to reported values of A ^{29,33,37}. The resulting variational magnetic phases coincide with the ones of Fig.3. Now F, zig-zag, CS, and IS settle near the $x-y$ plane, and the QP phase develops a uniaxial director vector along the $\hat{\mathbf{z}}$ axis. At $A \sim 1.4 \times 10^{-1} J_1$, the zig-zag phase settles in the $x-y$ plane, slightly inclined out of it by an angle ~ 8 degrees. The boundary between zig-zag and spiral phases moved slightly toward smaller K_1 and J_3 after the inclusion of easy plane anisotropy (as shown in the Supplementary Material).

Results from Monte Carlo simulations of an anisotropic Heisenberg model with first and third nearest neighbor interactions using ab-initio parameters support the hypothesis that a Neel order could compete with the zig-zag in NiPS₃²⁹. That could be the case if the nearest neighbour couplings J_1 were positive or if $J_1 < \frac{|K_1|}{2}$, which based in our calculations is not possible for this material: Table II shows K_1 to be about one order of magnitude smaller than J_1 in bulk; thus, a Neel state is unlikely to occur, at least in bulk NiPS₃. However for the case of monolayers where J_1 is positive, and K_1 is negative and much smaller than J_1 , the variational calculations confirm a Neel order (Supplementary Material).

Depending on the relative strength between the spin couplings, Eq.1 gives rise to four magnetic phases at $T=0$. The zig-zag phase, which has been found in bulk samples of NiPS₃, is the most likely to occur and competes with spiral magnetic patterns when we use the available values for Coulomb repulsion, Hund's coupling and d-p gaps from DFT calculations in the computed bulk spin exchange couplings. One aspect that has remained controversial is whether or not the zig-zag order survives up to the monolayer limit^{23,29}. Experiments suggest that the crystal field of bulk and monolayer NiPS₃ differs^{20,26,36} and here we assume that a consequence is that the active d orbitals in both cases have a different symmetry^{15,22,35,37}. Assuming that the angle between Ni and S atoms does not change due to the trigonal distortion in monolayers, we have shown that a possible consequence of that is the relative decrease of the spin couplings in monolayer systems. The positive and very small J_1 of monolayers (Table II) could drive samples toward a Neel phase, an IS or a disordered state. Which path monolayers will take it is unknown at this point: for such small J_1 , quantum fluctuations or interactions like second nearest neighbors could play a role and effects like disorder could become relevant⁵⁰. One important aspect not considered here is the deviation of the ninety de-

grees angle between Ni and sulfur atoms in monolayers³². According to Goodenough-Kanamori rules^{52,53}, such deviations could favor a superexchange mediated by a single p orbital, which would increase the magnitude of the antiferromagnetic J_1 in monolayer samples. If that were the case, the variational calculations show that a Neel order is favored in monolayers.

SUPPLEMENTARY MATERIAL

It contains details of calculations of the microscopic Hamiltonian and the perturbative approach to find the effective spin model. It also includes additional figures of variational spin correlations and magnetic phases.

ACKNOWLEDGMENTS

This work was supported by Fondecyt under Grant No. 1210083. The author thanks Je-Geun Park, Joerg Schmalian, and Alexander Mirlin for valuable discussions.

DATA AVAILABILITY STATEMENT

The data that support the findings of this study are available within the article [and its supplementary material].

- ¹K. S. Burch, D. Mandrus, and J.-G. Park, *Nature* **563**, 47 (2018).
- ²U. F. Seifert, M. Ye, and L. Balents, *Physical Review B* **105**, 155138 (2022).
- ³S. Y. Kim, T. Y. Kim, L. J. Sandilands, S. Sinn, M.-C. Lee, J. Son, S. Lee, K.-Y. Choi, W. Kim, B.-G. Park, et al., *Physical review letters* **120**, 136402 (2018).
- ⁴Y. Gu, Q. Zhang, C. Le, Y. Li, T. Xiang, and J. Hu, *Physical Review B* **100**, 165405 (2019).
- ⁵S. Rosenblum, A. Francis, and R. Merlin, *Physical Review B* **49**, 4352 (1994).
- ⁶S. Rosenblum and R. Merlin, *Physical Review B* **59**, 6317 (1999).
- ⁷R. Basnet, A. Wegner, K. Pandey, S. Storment, and J. Hu, *Physical Review Materials* **5**, 064413 (2021).
- ⁸D. Afanasiev, J. R. Hortensius, M. Matthiesen, S. Mañas-Valero, M. Šiškins, M. Lee, E. Lesne, H. S. van Der Zant, P. G. Steeneken, B. A. Ivanov, et al., *Science advances* **7**, eabf3096 (2021).
- ⁹C. A. Belvin, E. Baldini, I. O. Ozel, D. Mao, H. C. Po, C. J. Allington, S. Son, B. H. Kim, J. Kim, I. Hwang, et al., *Nature communications* **12**, 1 (2021).
- ¹⁰S. Kang, K. Kim, B. H. Kim, J. Kim, K. I. Sim, J.-U. Lee, S. Lee, K. Park, S. Yun, T. Kim, et al., *Nature* **583**, 785 (2020).
- ¹¹E. Ergeçen, B. Ilyas, D. Mao, H. C. Po, M. B. Yilmaz, J. Kim, J.-G. Park, T. Senthil, and N. Gedik, *Nature Communications* **13**, 98 (2022).
- ¹²X. Jiang, Q. Liu, J. Xing, N. Liu, Y. Guo, Z. Liu, and J. Zhao, *Applied Physics Reviews* **8** (2021).
- ¹³D. C. Mattis, *The theory of magnetism I: Statics and Dynamics*, vol. 17 (Springer Science & Business Media, 2012).
- ¹⁴H. J. Kim and K.-S. Kim, *New Journal of Physics* **25**, 083029 (2023).
- ¹⁵J. A. Wilson and A. Yoffe, *Advances in Physics* **18**, 193 (1969).
- ¹⁶R. Basnet, K. M. Kotur, M. Rybak, C. Stephenson, S. Bishop, C. Autieri, M. Birowska, and J. Hu, *Physical Review Research* **4**, 023256 (2022).
- ¹⁷K. F. Mak, J. Shan, and D. C. Ralph, *Nature Reviews Physics* **1**, 646 (2019).
- ¹⁸D. Lançon, R. Ewings, T. Guidi, F. Formisano, and A. Wildes, *Physical Review B* **98**, 134414 (2018).
- ¹⁹M. Kertesz and R. Hoffmann, *Journal of the American Chemical Society* **106**, 3453 (1984).
- ²⁰J. C. Hempel and M. E. Miller, *The Journal of Chemical Physics* **75**, 2959 (1981).

- ²¹S. Sugano, *Multiplets of transition-metal ions in crystals* (Elsevier, 2012).
- ²²E. Koch, Correlated electrons: from models to materials **2**, 1 (2012).
- ²³T. Y. Kim and C.-H. Park, Nano Letters **21**, 10114 (2021).
- ²⁴A. R. Wildes, V. Simonet, E. Ressouche, G. J. Mcintyre, M. Avdeev, E. Suard, S. A. Kimber, D. Lançon, G. Pepe, B. Moubaraki, et al., Physical Review B **92**, 224408 (2015).
- ²⁵A. Wildes, J. Stewart, M. Le, R. Ewings, K. Rule, G. Deng, and K. Anand, Physical Review B **106**, 174422 (2022).
- ²⁶K. Kim, S. Y. Lim, J.-U. Lee, S. Lee, T. Y. Kim, K. Park, G. S. Jeon, C.-H. Park, J.-G. Park, and H. Cheong, Nature Communications **10**, 1 (2019).
- ²⁷A. Scheie, P. Park, J. Villanova, G. Granroth, C. Sarkis, H. Zhang, M. Stone, J.-G. Park, S. Okamoto, T. Berlijn, et al., arXiv preprint arXiv:2302.07242 (2023).
- ²⁸B. L. Chittari, Y. Park, D. Lee, M. Han, A. H. MacDonald, E. Hwang, and J. Jung, Physical Review B **94**, 184428 (2016).
- ²⁹C. Lane and J.-X. Zhu, Physical Review B **102**, 075124 (2020).
- ³⁰A. Ushakov, D. Kukusta, A. Yaresko, and D. Khomskii, Physical Review B **87**, 014418 (2013).
- ³¹K. Hwangbo, Q. Zhang, Q. Jiang, Y. Wang, J. Fonseca, C. Wang, G. M. Diederich, D. R. Gamelin, D. Xiao, J.-H. Chu, et al., Nature Nanotechnology **16**, 655 (2021).
- ³²R. Brec, Solid State Ionics **22**, 3 (1986).
- ³³T. Olsen, Journal of Physics D: Applied Physics **54**, 314001 (2021).
- ³⁴N. Chandrasekharan and S. Vasudevan, Journal of Physics: Condensed Matter **6**, 4569 (1994).
- ³⁵W. A. Harrison, *Electronic structure and the properties of solids: the physics of the chemical bond* (Courier Corporation, 2012).
- ³⁶A. G. Chang, L.-W. Lan, Y.-J. Chan, C.-N. Kuo, T. Chen, C.-H. Huang, T.-H. Chuang, D.-H. Wei, C.-S. Lue, and C.-C. Kuo, Physical Review B **106**, 125412 (2022).
- ³⁷C. Autieri, G. Cuono, C. Noce, M. Rybak, K. M. Kotur, C. E. Agrapidis, K. Wohlfeld, and M. Birowska, The Journal of Physical Chemistry C **126**, 6791 (2022).
- ³⁸D. Klein and W. Seitz, Physical Review B **8**, 2236 (1973).
- ³⁹P. Van Dongen, Physical Review B **49**, 7904 (1994).
- ⁴⁰H.-J. Koo, R. Kremer, and M.-H. Whangbo, Molecules **26**, 1410 (2021).
- ⁴¹P. W. Anderson, Physical Review **79**, 350 (1950).
- ⁴²F. Mila and F.-C. Zhang, The European Physical Journal B-Condensed Matter and Complex Systems **16**, 7 (2000).
- ⁴³P.-O. Löwdin, The Journal of Chemical Physics **19**, 1396 (1951).
- ⁴⁴J. R. Schrieffer and P. A. Wolff, Physical Review **149**, 491 (1966).
- ⁴⁵S. Bravyi, D. P. DiVincenzo, and D. Loss, Annals of physics **326**, 2793 (2011).
- ⁴⁶M. Hoffmann and S. Blügel, Physical Review B **101**, 024418 (2020).
- ⁴⁷J. C. Slater and G. F. Koster, Physical review **94**, 1498 (1954).
- ⁴⁸A. Läuchli, F. Mila, and K. Penc, Physical review letters **97**, 087205 (2006).
- ⁴⁹B. A. Ivanov and A. K. Kolezhuk, Physical Review B **68**, 052401 (2003).
- ⁵⁰E. Stoudenmire, S. Trebst, and L. Balents, Physical Review B **79**, 214436 (2009).
- ⁵¹W. R. Inc., *Mathematica, Version 12.3*, champaign, IL, 2023, URL <https://www.wolfram.com/mathematica>.
- ⁵²J. B. Goodenough, Physical Review **100**, 564 (1955).
- ⁵³J. Kanamori, Journal of Physics and Chemistry of Solids **10**, 87 (1959).